GEMINI
8-M Telescopes Project

RPT-O-G0030

Primary Mirror Cell Deformation and Its Effect on Mirror Figure Assuming a Six-zone Axial Defining System

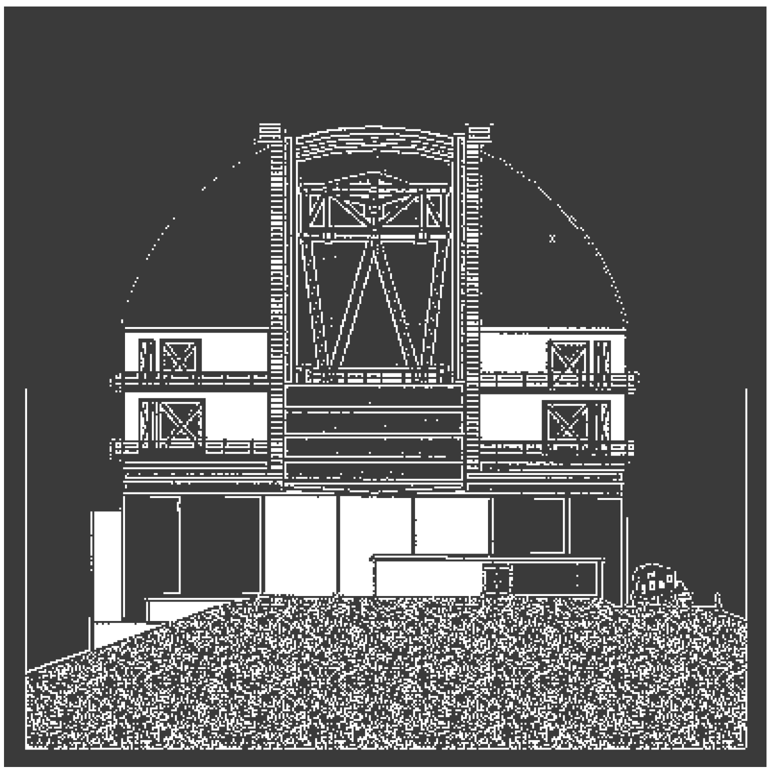

Larry Stepp
Optics Manager

Eugene Huang
Opto-structural Engineer

Eric Hansen
Opto-mechanical Engineer

November 1993

GEMINI PROJECT OFFICE 950 N. Cherry Ave. Tucson, Arizona 85719
Phone: (602) 325-9329 Fax: (602) 322-8590

Table of Contents

SECTION	Page No.
1. Executive Summary	1
2. Introduction	2
3. Error Budget	4
4. Effect Of Cell Deformations On Mirror Figure	5
5. Gravitational Flexure Of The Mirror Cell	7
6. Thermal Distortion	12
7. Affect Of Telescope Structure Deformation	15
8. Trade Study: 3-Bipod Vs 4-Bipod Cell Support	17
9. Conclusions	18
10. Acknowledgements	19

1. EXECUTIVE SUMMARY

This paper describes the effect on the mirror figure of mirror cell flexure, which can be partially transferred to the mirror by the six-zone axial defining system. The error budget allowance for this effect is small, and the calculations presented in this report show that it can be met at the worst case telescope orientation, with more than a factor of 4 margin on active optics cycle time.

The mirror cell design has been optimized to reduce gravity flexure, principally by extending the telescope center section under the cell to support it at a 60% radius. Two mirror cell support concepts are analyzed, a 3-bipod design and a 4-bipod design. Both could be made to work, but there is a larger performance margin with the 4-bipod design, so it has been adopted as the baseline design.

Seven analysis cases are presented that investigate the susceptibility to thermal effects in the mirror cell. For cases modeling realistic amounts of heat input at the known heat source locations in the mirror cell, the effects on the mirror are small compared to the effects of gravitational flexure.

The effect of twisting of the telescope structure is evaluated, for the 4-bipod cell support design. Only structural flexures that are anti-symmetric about both the X- and Y-axes (abbreviated AA) will bend the mirror cell. Three analysis cases are presented investigating: (1) uncontrolled torque from the elevation drives; (2) wind-induced flexure at a wind speed of 11 m/sec and worst case wind orientation; and (3) thermal effects in the center section. No heat sources having AA symmetry are currently planned or anticipated to be located in the center section. Provided that large AA heat inputs are avoided, the effects of telescope structure twisting should be negligible.

The rate of change of mirror figure at worst case tracking rates will introduce only small errors in the active optics wavefront sensing; these errors are consistent with the wavefront sensor error budget.

2. INTRODUCTION

The Gemini primary mirror support can be operated in several modes, including one mode in which the distributed defining system is divided into six zones. The six-zone defining system resists wind loading better than a kinematic system, because the mirror is coupled to the stiffness of the mirror cell. By constraining three degrees of freedom more than a kinematic defining system does, three orthogonal bending modes of the mirror are coupled to the cell. This is described in the Gemini technical report, *The Distributed Defining System for the Primary Mirrors*.

When the support is in the six-zone mode, deformation of the mirror cell can bend the mirror because of this kinematic overconstraint. The three possible modes of mirror bending are all easily corrected with the active optics system, however, the frequency required for active optics corrections will depend on the rate at which the mirror cell changes shape. Studies of wavefront sensor characteristics indicate integration times of approximately 60 seconds will be required to average out atmospheric seeing, and to ensure a 99% probability that there will be a bright enough star within the field, even at the north galactic pole. If the mirror cell changes shape too rapidly, two adverse effects could occur. First, the accuracy of the wavefront sensing could be affected, and second, the error budget for mirror support errors might be exceeded in less time than one correction cycle.

Only a small amount of the Gemini error budget has been allowed for this effect. In order to keep it one of the smaller terms in the error budget, we have designed the mirror cell to avoid rapid structural deformation during telescope operation. This deformation could come from three different sources: (1) the effect of changing gravity orientation on the telescope structure including the mirror cell, (2) the effect of non-uniform temperatures on the mirror cell structure, and (3) any other deformations of the telescope structure that are transferred to the mirror cell. Each of these possible effects is discussed in a later section of this report.

To minimize the gravity sag of the cell, we have adopted the philosophy of supporting the cell as though it were a mirror. Therefore, the axial support of the cell is at a 60% radius, and the lateral support is applied close to the center of gravity of the entire primary mirror assembly. This type of support for the cell reduces the deformation under gravity by approximately a factor of four. To provide support for the cell in this way, the telescope center section has been extended underneath the cell.

To follow the philosophy of supporting the cell as though it were a mirror, in principle we should provide a kinematic support between the telescope structure and the cell. This can be accomplished by supporting the cell on six struts, arranged as three bipods. An alternative is to support the cell in a more traditional way, on eight struts arranged as four bipods. These two concepts are illustrated in **Figure 1**. In this report the amount of cell bending from gravity sag, thermal expansion, and telescope structure flexure will be calculated for both 3-bipod and 4-bipod designs. Section 8 will summarize the relative merits of these two approaches.

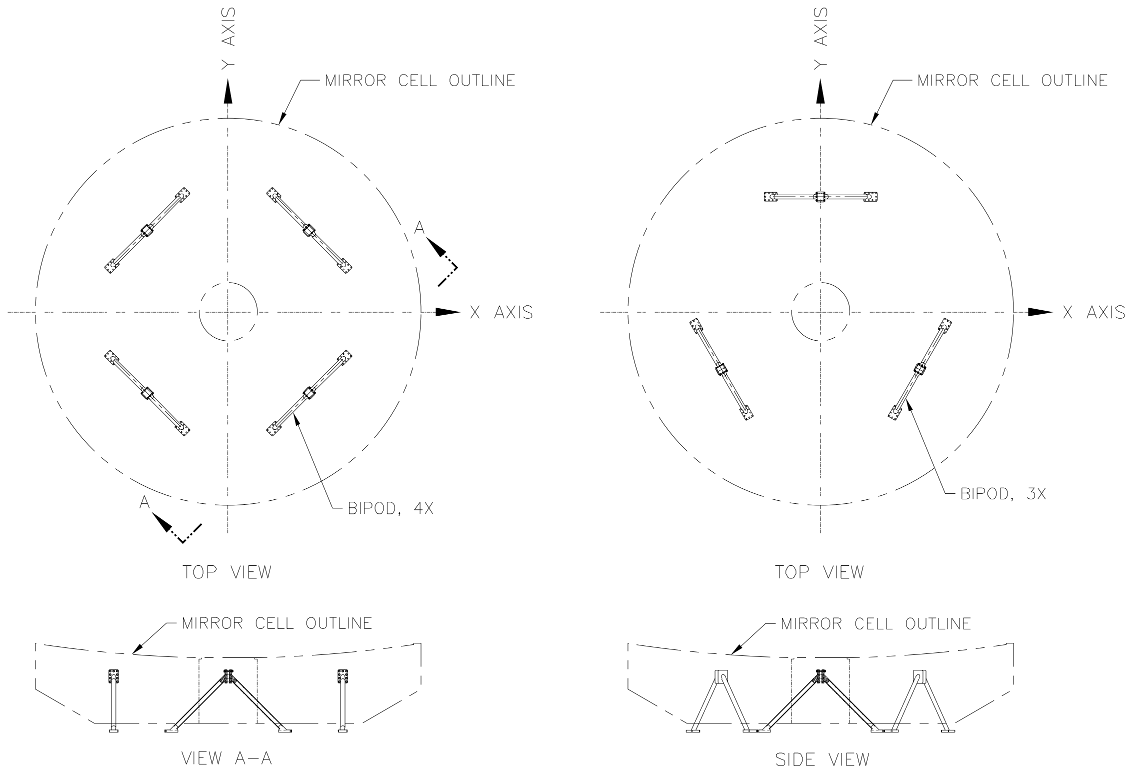

Figure 1. Schematic diagrams of the two mirror cell support concepts.

2.1. Coordinate Systems

The coordinate system used in this report is a right-handed Cartesian system with the origin at the vertex of the primary mirror. The Z-axis is the telescope optical axis, with the positive direction pointing from the primary mirror towards the secondary mirror. The X-axis is parallel to the telescope elevation axis and the Y-axis is in the lateral direction that points to the zenith when the optical axis is pointing to the horizon. The zenith angle θ_Z is the angle between the zenith and the optical axis.

The line of action of the axial support mechanisms is in a direction that points towards the center of curvature of the mirror. This direction is normal to (that is, perpendicular to) the back of the mirror, and in terms of local coordinates is defined as the "normal direction".

The orientation of the six support zones relative to the coordinate axes is shown in **Figure 2.**

Figure 2. Orientation of the six support zones relative to the coordinate axes.

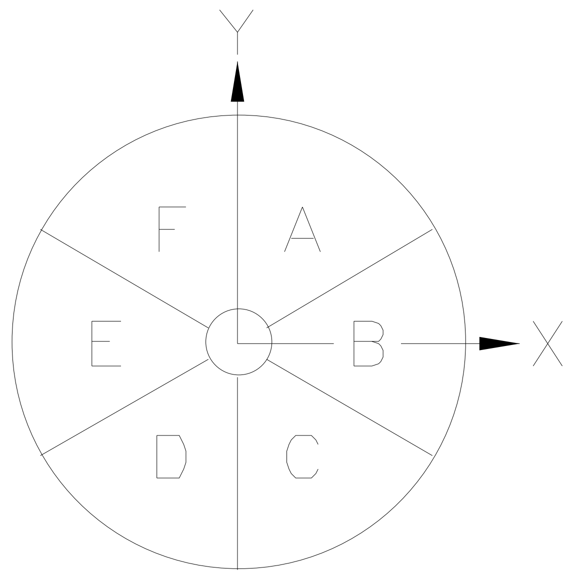

3. ERROR BUDGET

The error budget for mirror deformation caused by the six-zone defining system is included in the error budget category for primary mirror support. The breakdown of the mirror support error budget is discussed in the Gemini technical report, *Response of Primary Mirror to Support System Errors*. A description of the complete error budget for the primary mirror assembly is included in the report *Summary of the Error Budget as it Affects the Primary Mirror Assembly.*

The error budget allows certain errors to increase as a function of zenith angle, and the effect of the six-zone defining system are in this category. **Figure 3** shows the amount the image diameters for 50% and 85% encircled energy are allowed to increase because of this effect. Because we know the specific aberration terms produced by this effect, the error budget has been adjusted so that the 50% and 85% budgets require equivalent figure accuracy, therefore the 50% error budget will be used as the criterion throughout the remainder of this report.

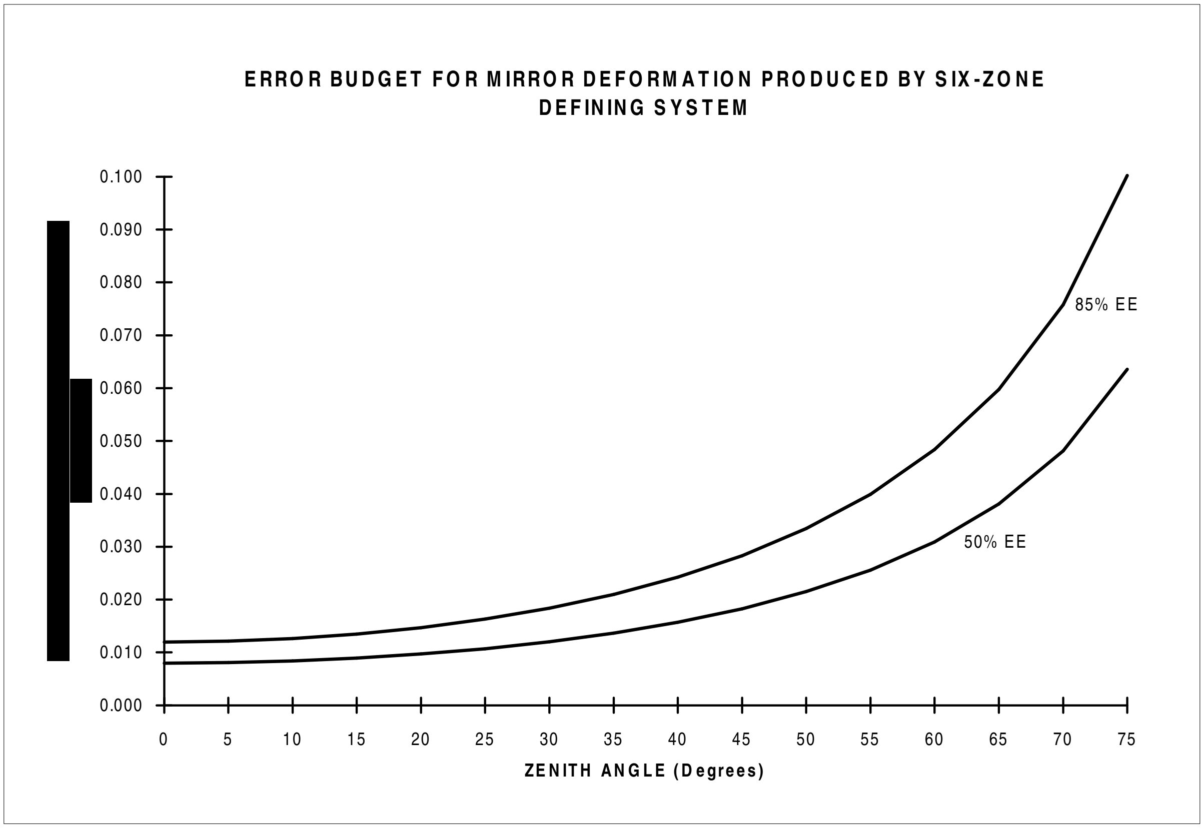

Figure 3. The error budget for mirror deformation caused by mirror cell bending coupled through the six-zone defining system, as a function of zenith angle, expressed in terms of encircled energy diameter increase at a wavelength of 2.2 μ**m.**

For the optical aberrations produced by the effects of the six-zone defining system, which are dominated by astigmatism, the approximate correlation between encircled energy at 2.2 μm wavelength and mirror surface distortion is:

0.01 arc second increase in 50% encircled energy ≈ 22 nm RMS

4. EFFECT OF CELL DEFORMATIONS ON MIRROR FIGURE

The coupling between the mirror and cell is through the axial defining system. In the six-zone mode, the 120 support points are divided into six zones having 20 points in each. Ignoring the elasticity of the components in the support system, the enclosed volume of "incompressible" fluid in each support zone will determine the average height of the hydraulic support mechanisms in that zone. In this sense, the mirror can be thought of as resting on six virtual fixed points, equally spaced around a circle. However, if component elasticity is considered, each zone of supports actually has a spring constant. The design value for individual mechanism stiffness is 8.8 N/µm, yielding a zonal stiffness of 176 N/µm. Therefore, the mirror should be thought of as resting on six virtual stiff springs.

When the mirror cell deforms, the pressures in the six hydraulic zones change, causing changes in the forces exerted on the mirror by the supports. The force changes will bend the mirror, and the support mechanisms will also change length slightly. Within any one support zone the force exerted on the mirror at each of the 20 locations in that zone will be determined by the hydraulic pressure, and will therefore be in proportion to the areas of the pistons.

The change in hydraulic pressure is determined by the average deflections at the support attachment points. It does not matter whether one support is moved 20 nm or 20 supports are moved one nm each--the effect on the mirror is the same. Therefore, to calculate the effect of cell bending on the mirror, it is necessary and sufficient to know the average deflections in the normal direction of the mirror cell structure at the 20 support points in each zone. These six average zonal deflection values determine the mirror bending.

Finite-element studies have shown that the cell is much stiffer than the mirror, therefore the bending of the cell can be calculated without considering the stiffness of the mirror (the difference in calculated deflections is less than 5%). However, the expected stiffness of the support mechanisms is less than an order of magnitude larger than the bending stiffness of the mirror. Both mirror and mechanism stiffnesses must be considered to determine the effect of mirror cell flexure on the mirror. In general, the stiffer the support mechanisms the greater will be the effect of cell bending on the mirror. Analysis has shown that if the support mechanisms were infinitely stiff, the deflections would be a factor of 1.6 times larger than for the design stiffness of 8.8 N/µm. The weight of the primary mirror has been included in the model used to calculate gravity flexure, as has the weight and moment of the Cassegrain instrument assembly.

The finite-element analysis described in this report has been done using the I-DEAS program from Structural Dynamics Research Corporation. One of the available features in I-DEAS is the use of a multiple-point constraint (MPC). When an MPC is used, the summation of displacements of a given set of nodes in the model equals zero. This constraint is ideal for modeling a hydraulic distributed defining system. To incorporate finite actuator stiffnesses, each support mechanism is modeled as a strut with a spring constant of 8.8 N/µm. The struts are oriented with their long axes normal to the mirror surface. The struts rest on the MPC, and the mirror is supported on the struts. In the finite-element model nine MPC's are used, six to model the axial defining system and three to model the lateral defining system.

Using finite-element analysis, influence coefficients have been determined for unit displacement of the cell structure under each of the six zones in the support system. These influences have been evaluated using Zernike polynomials. As described in the report on *The Distributed Defining System for the Primary Mirrors*, only three Zernike terms are produced in any significant amount by the six-zone system: two orientations of astigmatism, and one orientation of trefoil. These correspond to the symmetry cases SS, AA and SA respectively. The influence coefficients for the six unit cases are given in **Table 1.**

CASE NO.	MIRROR CELL ZONAL AVERAGE DISPLACEMENTS (nm)						MIRROR DEFORMATION (nm RMS)			
	A	B	C	D	E	F	SS	AA	SA	TOTAL
1	1000	0	0	0	0	0	-106	184	-60	227
2	0	1000	0	0	0	0	212	0	60	226
3	0	0	1000	0	0	0	-106	-184	-60	225
4	0	0	0	1000	0	0	-106	184	60	225
5	0	0	0	0	1000	0	212	0	-60	226
6	0	0	0	0	0	1000	-106	-184	60	227

Table 1. Primary mirror deformation, in terms of the three characteristic aberration mode shapes, from zonal unit cases of mirror cell flexure. Total column includes 36 Zernike terms.

Although only three Zernike terms are produced at a significant level, all calculations described below included 36 Zernike terms, to avoid any loss of accuracy.

An influence coefficient matrix was produced from the cell deflection unit cases. Each column in the matrix is the list of mirror deformation Zernike coefficients for one of the six unit cases. For any change in mirror cell shape calculated by finite-element analysis, the average displacements are determined for each of the six zones. The vector consisting of these six average displacements is multiplied by the influence coefficient matrix to determine the mirror deformation that would result from the mirror cell deflections. This deformation is expressed in terms of a list of 36 Zernike coefficients.

5. GRAVITATIONAL FLEXURE OF THE MIRROR CELL

As the telescope tracks across the sky the zenith angle changes continuously. The changing gravity vector direction relative to the cell causes deformation of the cell, which not only has to support its own weight but also has to carry the primary mirror and the instruments at the Cassegrain focus. Our design goal is to minimize the rate of change of mirror cell shape as the telescope tracks across the sky, by minimizing the gravitational flexure of the cell.

The rate of change of cell shape during slewing is not an issue here, because no observations are made and because the defining system will be changed into a kinematic three-zone system (by opening three valves) to allow for the more rapid mirror cell flexure that will occur. In any case, as will be shown below, the maximum mirror deformation that could occur during slewing is only a few microns, even if the defining system were kept in its six-zone mode. This is still within the analysis range of the wavefront sensor.

The rate at which the zenith angle changes during tracking depends on the position in the sky of the object being observed. For an alt-azimuth telescope, the path across the sky for which the rate of change of zenith angle is maximum for all zenith angles is the one that passes through the zenith. **Figure 4** shows the rate of change of zenith angle as a function of hour angle for tracking an object through the zenith, for a telescope on Mauna Kea. Note the maximum rate of change is just under 0.004 degree per second. As a conservative worst case assumption, we will assume a rate of change of zenith angle of 0.004 degree per second, for all zenith angles.

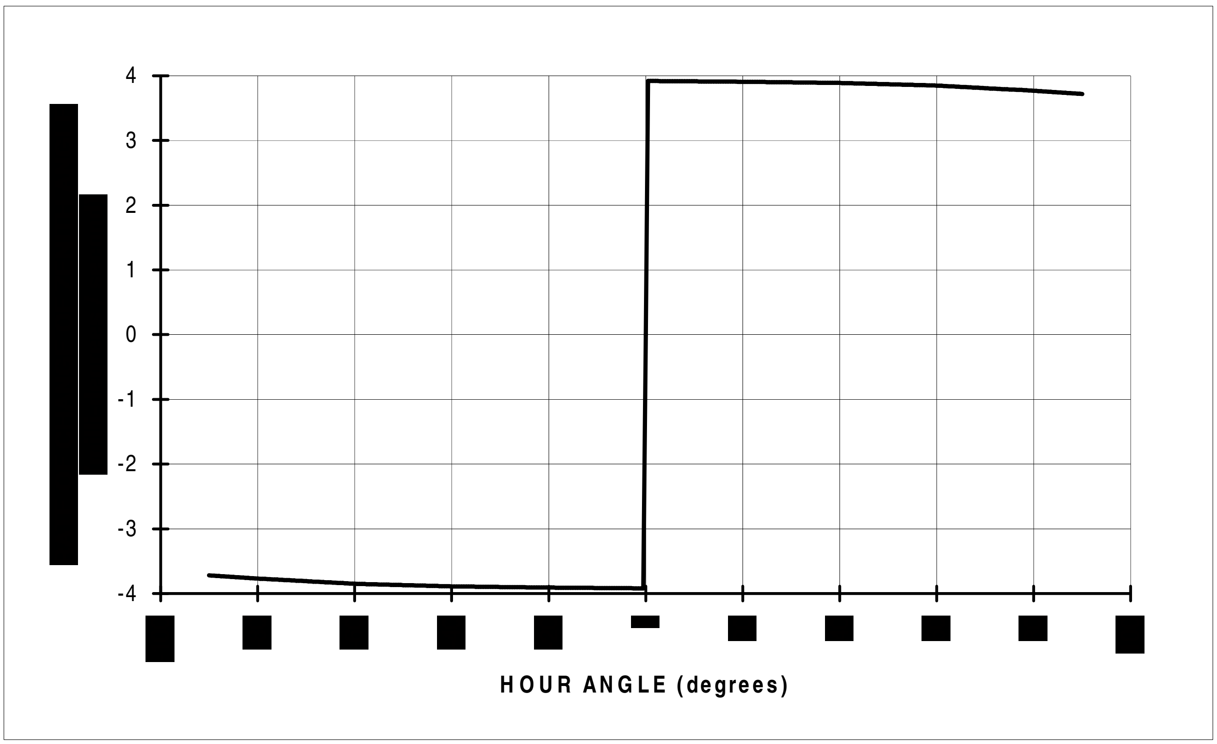

Figure 4. The rate of change of zenith angle as a function of hour angle, for tracking an object through the zenith, on Mauna Kea. This path requires the maximum rate of zenith angle change during tracking for all zenith angles.

The gravitational flexure of the mirror cell can be divided into two orthogonal parts, corresponding to the flexure experienced at zenith pointing, and the flexure experienced at horizon pointing. As the telescope changes zenith angle, the zenith pointing component varies as the $\cos(\theta_Z)$. The horizon pointing component varies as the $\sin(\theta_Z)$. Therefore, the total deflection at any angle between the zenith and horizon can be determined by the superposition of the zenith-pointing deflection multiplied by the cosine of the zenith angle, plus the horizon-pointing deflection multiplied by the sine of the zenith angle.

Note that the rate of change of the zenith-pointing component varies as the derivative of cos(θ_Z), or -sin(θ_Z), while the rate of change of the horizon-pointing component varies as cos(θ_Z).

5.1. Gravitational flexure of the 3-bipod design

Figure 1 shows that the 3-bipod support is symmetric about the Y-axis but not about the X-axis. The chosen locations for the three bipods, 120° apart, are aligned with the joints between mirror support zones. The gravity deflections of the mirror cell have 120° symmetry, therefore, the average displacements of the six mirror support zones are equal for the zenith pointing case. This means the zenith-pointing cell deflections have almost no effect on the mirror figure. The zenith-pointing and horizon-pointing gravity deflections of the top surface of the mirror cell on the 3-bipod support are shown in **Figure 5**.

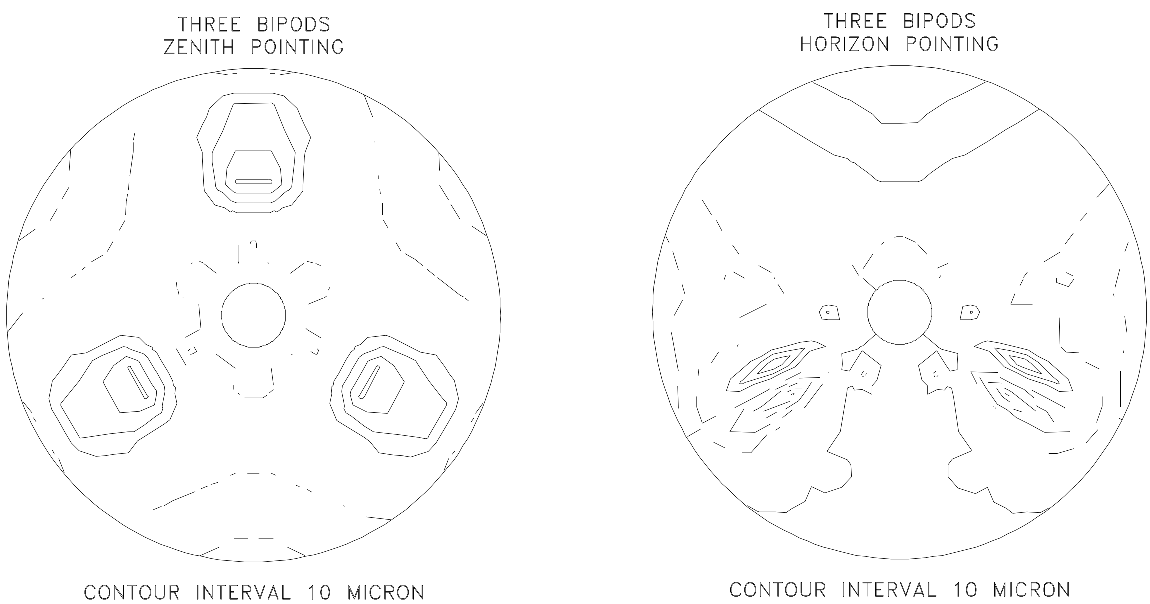

Figure 5. Gravitational deflections of the top surface of the mirror cell on the 3-bipod support.

The average deflections of each of the six zones has been calculated for these two cases. **Table 2** contains information about the average zonal deflections and the associated mirror deformations for each case. Tilt and piston have been removed from the numbers.

5.1.1. Rate of Change With Zenith Angle: 3-Bipod Cell Support

Because there is almost no mirror deformation from the zenith-pointing component of cell flexure, the rate of change of mirror deformation varies as the cosine of the zenith angle. **Figure 6** shows the increase in encircled energy diameter caused by the amount of mirror deformation that would occur in one minute because of the six-zone defining system. Note that for longer times between active optics updates, the error budget would be exceeded first at the zenith.

CASE	MIRROR CELL ZONAL AVERAGE DISPLACEMENTS (nm)						MIRROR DEFORMATION (nm RMS)			
	A	B	C	D	E	F	SS	AA	SA	TOTAL
3-Bipod Zenith	1	-1	1	1	-1	1	1	0	0	1
3-Bipod Horizon	2007	-4013	2006	2007	-4012	2006	2573	0	0	2611

Table 2. Average mirror cell zonal displacements and mirror deformations produced by the two orthogonal components of gravitational flexure, for the design with 3 bipods supporting the mirror cell. The number in the total column includes 36 Zernike terms.

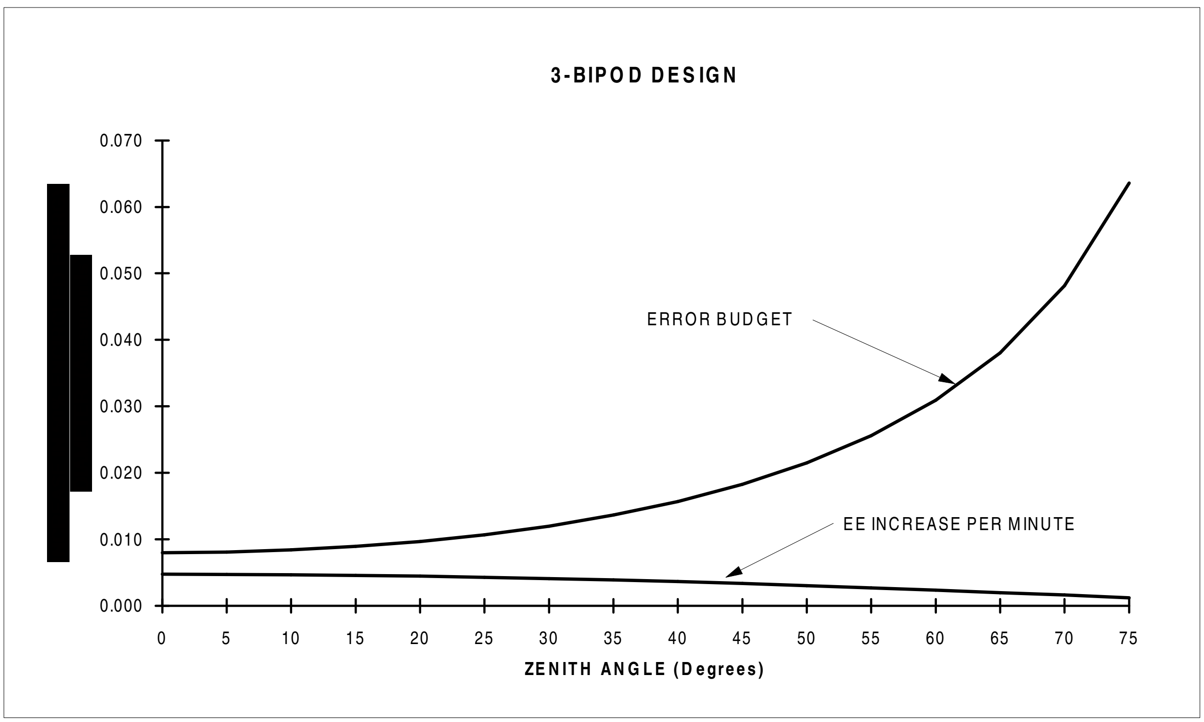

Figure 6. A comparison between the error budget for increase in 50% encircled energy diameter and the amount of image spread caused by one minute of tracking, at the worst case elevation tracking rate, without active optics correction, for the 3-bipod design.

5.2. Gravitational flexure of the 4-bipod design

The zenith-pointing and horizon-pointing gravity deflections of the mirror cell on the 4-bipod support are shown in **Figure 7.** The 4-bipod cell support produces cell deformations with a four-fold character at zenith pointing. This deformation affects the six mirror support zones differently, producing astigmatism in the mirror. The horizon-pointing cell deformations are anti-symmetric about the X-axis, since the structure is symmetric and the applied loads are anti-symmetric. Because of the chosen orientations of the six mirror support zones, this anti-symmetric deformation produces only rigid-body tilt of the mirror. The two upper support zones have unit positive displacement, the two middle zones have zero displacement, and the two lower zones have unit negative displacement. The mirror figure is not distorted by the 4-bipod horizon-pointing cell flexure.

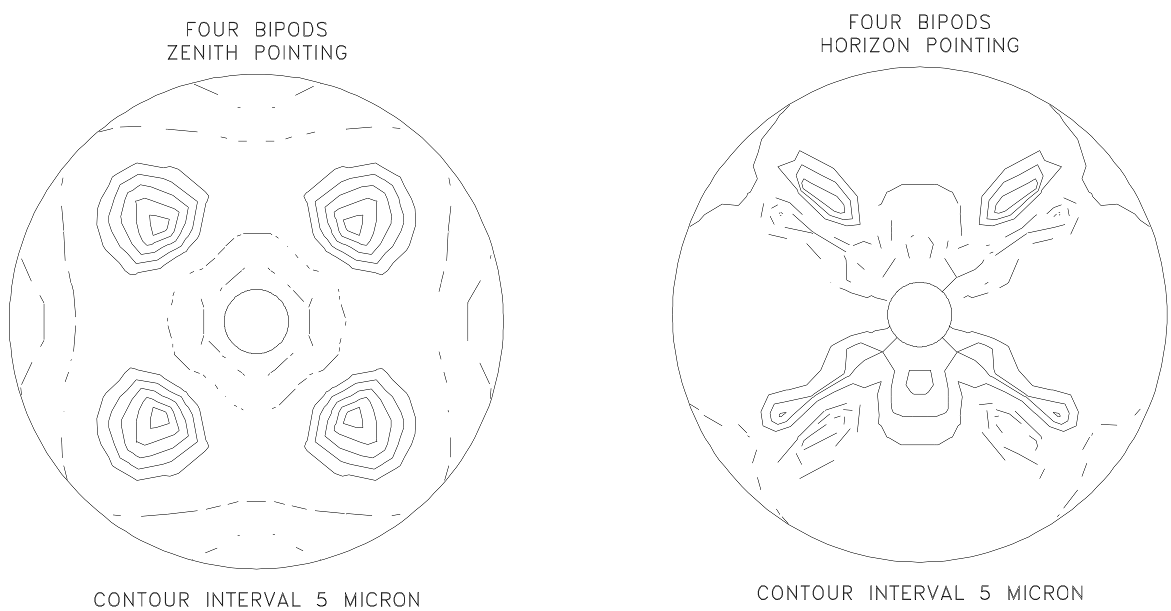

Figure 7. Gravitational deflections of the mirror cell on the 4-bipod support.

The 4-bipod cell support is slightly overconstrained, therefore the cell could be bent by deformation of the telescope structure. However, for the case of changing gravity orientation, all telescope deformations will be symmetric about the Y-axis. The orientation of the four bipods at 45° from the telescope elevation axis ensures that, for telescope structural deformations symmetric about the Y-axis, telescope deformations that are *either* symmetric or anti-symmetric about the X-axis will not distort the cell. The only telescope structural deformations that could affect the mirror cell are those that are anti-symmetric about both the X- and Y-axes. This type of effect is described in Section 7.

The average deflections of each of the six zones has been calculated for these two cases. **Table 3** contains information about the average zonal deflections and the associated mirror deformations from each case. Tilt and piston have been removed from the average zonal deflections.

CASE	MIRROR CELL ZONAL AVERAGE DISPLACEMENTS (nm)						MIRROR DEFORMATION (nm RMS)			
	A	B	C	D	E	F	SS	AA	SA	TOTAL
4-Bipod Zenith	1725	-3449	1725	1725	-3449	1725	2211	0	0	2255
4-Bipod Horizon	5	-7	4	8	-16	6	7	0	1	8

Table 3. Average mirror cell zonal displacements and mirror deformations produced by the two orthogonal components of gravitational flexure, for the design with 4 bipods supporting the mirror cell. The number in the total column includes 36 Zernike terms.

5.2.1. Rate of Change With Zenith Angle: 4-Bipod Cell Support

Because there is almost no mirror deformation from the horizon-pointing component of cell flexure, the rate of change of mirror deformation varies as the sine of the zenith angle. **Figure 8** shows the increase in encircled energy diameter caused by the amount of mirror deformation that would occur in one minute because of the six-zone defining system. For longer times between active optics updates, the error budget would be exceeded first at a zenith angle of 30 degrees after approximately six minutes.

6. THERMAL DISTORTION

Deflection of the cell structure could also be caused by thermal effects. A number of components of the primary mirror assembly could transfer heat to or from the steel cell. These components include:

- The control electronics housed in a VMS crate, mounted in the cell
- The Cassegrain rotator bearing, and scientific instruments
- The radiation plate for the mirror thermal control system
- The active optics actuators

A number of analysis cases have been run to investigate the effects of potential heat transfer situations. The TMG package from MAYA Heat Transfer Technologies Ltd. was used with I-DEAS finite-element models to calculate heat transfer in the mirror cell. The resulting thermal distributions were applied to the structural model, and the flexure of the cell was calculated.

Figure 8. A comparison between the error budget for increase in 50% encircled energy

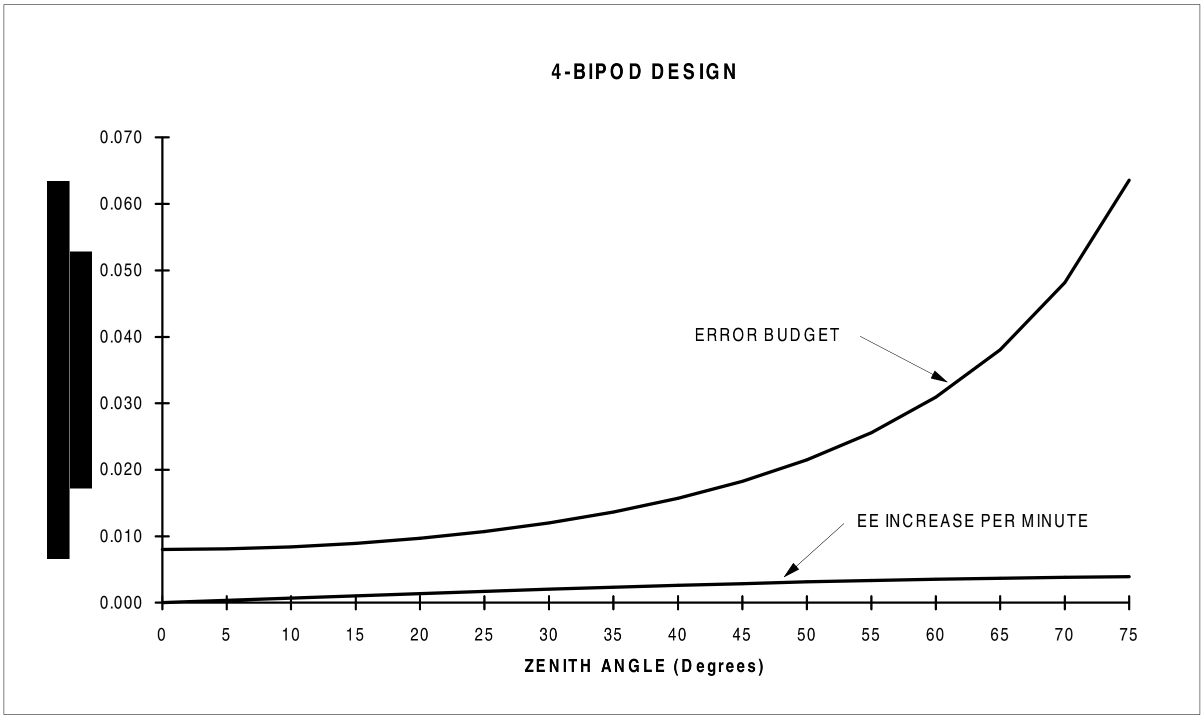

diameter and the amount of image spread that would be caused by one minute of tracking, at the worst case elevation tracking rate, without active optics correction, for the 4-bipod design.

The thermal cases fall into two categories. Some of the cases evaluated conditions in which a heat load or sink was applied to the cell. In these cases, the highest rate of change occurred during the first part of the time interval, and the rate of change at the end of the night was typically 20 to 30% lower. Other cases evaluated conditions in which the changing night-time temperature affected the cell. In those cases the rate of change was highest at the end of the night, when the largest temperature differences occurred. In calculating the results presented in this report, the worst 5 minute period was considered for each case.

The following cases have been evaluated:

Case 1. This case was used to confirm the performance of the model. A one degree gradient was applied to the cell structure, with the rear surface at 0 degrees and the front surface at 1 degree. This was compared to the closed form solution for a disk subjected to a linear gradient, for which:

$$W_{P\text{-}V} = r^2\alpha\Delta T/2h$$

where: r = radius of mirror cell
h = mirror cell thickness
α = coefficient of thermal expansion

The closed form solution gave a cell top surface deflection of 82 µm P-V, as compared to the FEA solution which yielded 88 µm. Because this case is rotationally symmetric, it had no effect on the mirror, since the six-zone defining system is not affected by rotationally symmetric cell deflections.

Case 2. This case represents a uniform radial gradient, from 0° at the optical axis to 1° at the outer edge of the cell. The P-V deformation of the mirror cell top surface was 3.9 microns. This case is also rotationally symmetric, and therefore has no effect on the mirror.

Case 3. This case modeled the effect of uneven cooling from wind ventilation. One side of the mirror cell was exposed to heat transfer and the other side was assumed to be perfectly insulated. The ambient air temperature declined from 1.8° C to 0.2° C during the night and the convective heat transfer coefficient was assumed to be 4.0 W/m^2K, which roughly corresponds to a 2 m/sec wind flowing past the side of the cell. This case is believed to be conservative, since the cell is closely surrounded by the telescope center section, which would shield its side from the wind and transfer heat to it by radiation if a temperature difference arose. For this case, the rate of change was highest at the end of the night. Results for this case are included in **Table 4**.

Case 4. This case modeled the heat input from an electronics enclosure holding a VME crate mounted within the mirror cell close to the outer edge. The engineer in the Telescope Group responsible for removing excess heat from telescope components has estimated that the heat leakage from this enclosure can be held to 10 watts. To be conservative, we modeled a heat input to the cell of 30 watts. The rate of change was highest for this case at the start of the time period. Results for this case are included in **Table 4**.

Case 5. This case models the heat transferred to the cell structure from the Cassegrain instrument rotator bearing. The rotator motors and scientific instruments are not attached directly to the cell, and it is planned that their heat output will be removed by the telescope cooling system. This case modeled a 50 watt residual heat leak into the cell from these sources. The heat was applied evenly around the bearing attachment points. For this case, the rate of change was highest at the start. Results for this case are included in **Table 4.**

Case 6. This case modeled the effect of the temperature difference produced by the mirror thermal control system. The maximum temperature difference of the radiation plate from the ambient temperature has been defined as ±15° C. The radiation plate will be separated from the cell structure by 50 mm of polystyrene foam insulation. For a temperature difference of 15 C, the heat flow would be 7.5 W/m2. The rate of change was highest for this case at the start of the time period. This case is believed to be conservative, because there will be ambient temperature cooling water loops in the top level of the mirror cell to remove heat from the active optics actuators, and those loops would help reduce the effects of radiation plate temperatures. However, this effect was not included in this model. Results for this case are included in **Table 4**.

Case 7. This case models the heat input to the cell from the 192 active optics actuators. With their associated electronics, they will dissipate approximately 5 watts each. Although there will be a cooling system that pumps ambient temperature water to heat sinks at each actuator, this case modeled 1 watt per actuator of residual heat applied to the cell structure. For this case, the rate of change was highest at the start. Results for this case are included in **Table 4**.

As can be seen from **Table 4**, the amount of mirror figure change from a five minute period of thermal bending of the cell is small for all the cases studied. This is because most of these cases produce primarily a uniform curvature change in the cell top surface, which is not transferred to the mirror by the six-zone support.

CASE NUMBER	MIRROR CELL ZONAL AVERAGE DISPLACEMENTS PER MINUTE (nm)						MIRROR DEFORMATION PER MINUTE (nm RMS)			
	A	B	C	D	E	F	SS	AA	SA	TOTAL
Thermal 3	0	0	0	0	0	0	0	0	0	0
Thermal 4	2	-4	2	2	-4	2	2	0	0	2
Thermal 5	0	0	0	0	0	0	0	0	0	0
Thermal 6	0	0	0	0	0	0	0	0	0	0
Thermal 7	0	-1	0	0	1	0	0	0	0	0

Table 4. Average mirror cell zonal displacements and mirror deformations produced by the thermal distortion cases. The numbers represent the change that would occur during a five minute period, at the worst part of the night for each case. Tilt and piston have been removed from the average zonal displacements. The number in the total column was calculated using 36 Zernike terms. Zeroes represent numbers smaller than 0.5 nm.

7. AFFECT OF TELESCOPE STRUCTURE DEFORMATION

The 3-bipod cell support would be essentially kinematic. In this design, flexure of the telescope structure would not cause mirror cell bending. The 4-bipod cell support is slightly overconstrained and could be affected by telescope flexure. Several analysis cases have been run to investigate this effect.

As mentioned in Section 5, the chosen orientation for the four bipods will prevent gravity flexure of the telescope structure from bending the mirror cell. Only telescope deflections that are anti-symmetric about both the X- and Y-axes can bend the cell. Several effects could be possible sources of this type of twisting telescope flexure.

One possible source of telescope twisting could be a malfunction of the elevation axis drives. The two drive systems will be controlled to divide the load evenly, but errors in the control system could conceivably cause a torque difference. The absolute worst case scenario was evaluated. The maximum possible opposed torque that could be produced by the four drive motors, 17430 N-m, was applied at the elevation axis. The results of this case are presented in **Table 5**. In reality, the unbalanced torque would be at least two orders of magnitude smaller than this.

Another possible source of telescope twisting is the wind. The worst wind orientation for anti-symmetric twisting of the structure would be a wind direction at 45 degrees to the elevation axis. A steady state wind velocity of 11 m/sec was modeled. The results of this case are presented in **Table 5.**

A third possible source of telescope twisting is thermal. No currently planned equipment in the telescope center section would produce any thermal effects that are anti-symmetric about both the X- and Y-axes. Since there is no anticipated heat load of this type to analyze, it was decided to try to identify areas with the greatest susceptibility to a heat input. This type of study would indicate upper limits that should be maintained for inadvertent heat loads on susceptible areas.

One area in the telescope structure where localized heating could distort the mirror cell is at the bipod struts. Thermal expansion of these struts would be directly coupled to bending of the mirror cell, with a relatively large lever arm to strengthen the effect. A 10 watt heat input to one of the struts was modeled and heat transfer out of the strut was neglected, so it would be subject to the full effect of the temperature rise. The results of the finite-element analysis case are included in **Table 5**. In reality, the strut is completely surrounded by reinforcing plates in the cell structure, and there is no planned heat source close to the struts, so this type of heat input is considered improbable.

Because of the stiffness of the telescope center section and mirror cell, mirror deformation caused by twisting of the telescope structure will be limited to the range of 1 or 2 nm per minute, provided that large heat sources are not located in particularly susceptible areas of the telescope center section.

CASE NUMBER	MIRROR CELL ZONAL AVERAGE DISPLACEMENTS (nm)						MIRROR DEFORMATION (nm RMS)			
	A	B	C	D	E	F	SS	AA	SA	TOTAL
Elevation drives (absolute worst case)	15	0	-15	15	0	-15	0	11	0	12
10 m/sec wind loading, worst orientation	-2	0	2	-2	0	2	0	2	0	2
Change caused per minute by 10 watts heat input to bipod strut	3	-3	1	3	-3	1	-2	1	0	2

Table 5. Results of FEA cases to investigate mirror cell bending caused by twisting of the telescope structure. The *elevation drives* case reflects the maximum effect that could be produced if the two elevation drives exerted their full torque in opposition to each other; the actual torque control will be at least a factor of 100 better than this.

8. TRADE STUDY: 3-BIPOD VS 4-BIPOD CELL SUPPORT

The principle performance differences between the 3-bipod and 4-bipod designs relate to the rate of change of gravitational flexure relative to the error budget, and the susceptibility to twisting of the telescope center section. **Table 6** summarizes these effects.

If cell thermal distortion and telescope twisting effects are added in quadrature with the effects of gravity, the 3-bipod design would remain within the error budget for about 1.6 minutes without active optics correction at the worst case telescope orientation, while the 4-bipod design would remain within the error budget for about 4.8 minutes without active optics correction at the worst case telescope orientation.

We believe the 3-bipod design could be made to work. The mirror cell structural design could be optimized to reduce the specific effects caused by gravity on the 3 bipod support. Also a feed-forward control system, using look up tables, could be used to make continuous corrections between active optics updates. However, it appears the 4-bipod design has more margin, and that design has been chosen as the Gemini baseline.

EFFECT	3-BIPOD DESIGN	4-BIPOD DESIGN
Worst case zenith angle for gravitational flexure, relative to the error budget	zenith	30 degrees
Error budget for mirror flexure at the worst case zenith angle	17 nm	26 nm
Predicted mirror figure change per minute from gravitational flexure during tracking, for the worst case tracking rate and zenith angle	10 nm	4 nm
Predicted mirror figure change per minute from mirror cell thermal effects	3 nm RMS	3 nm RMS
Predicted mirror figure change per minute from twisting of the telescope structure	0	2 nm RMS

Table 6. A comparison between the performance of the 3-bipod and 4-bipod cell support designs. The principal advantage of the 4-bipod design is that its gravitational flexure has its maximum and minimum values at the same zenith angles as the error budget (see Figure 8).

9. CONCLUSIONS

This report has investigated expected deformation of the mirror cell and its effect on the figure of the primary mirror if the defining system is used in the overconstrained six-zone mode.

The mirror cell and its supporting structure have been designed to minimize the gravity flexure of the cell. The 4-bipod cell support has been chosen because its flexure is somewhat smaller, and it fits the error budget better than the 3-bipod design. Calculations show that the slight overconstraint inherent in the 4-bipod design will not cause significant problems, provided that large heat loads are not applied at particularly susceptible locations in the telescope center section structure. No heat loads of this type are planned or anticipated.

In general the change in mirror figure is smaller than the amount of mirror cell flexure that caused it. This is because there is only a slight overconstraint between the mirror and cell, and only differences in average zonal displacements of the support attachment points on the cell structure have an influence on the mirror. Many types of cell flexure have no influence on the mirror figure, including:

- piston
- tilt
- any rotationally symmetric flexures
- any flexures that are anti-symmetric about the X-axis
- flexures with 60° symmetry

9.1 Length of time between active optics updates

The predicted allowable time period between active optics updates is longer than 4.5 minutes in the worst case orientation. This compares to an anticipated wavefront sensor integration time of 60 seconds. Gravitational flexure of the cell is expected to cause more rapid effects than thermal distortions and the effect of telescope structural twisting at all zenith angles above about 20 degrees.

9.2 Ability to increase performance with open loop corrections

Most of the effects that have been discussed in this report are continuous, and increase or decrease monotonically over relatively long time periods. Therefore, it should be possible to design a feed-forward control system that can learn which direction the cell is bending, and apply gradual open loop mirror support corrections that anticipate the cell flexure. With the use of this type of control system, it is anticipated that the length of time between active optics updates for control of the effects of cell bending could be increased by a factor of 5 to 10.

9.3 Effect on Wavefront Sensor Accuracy

The rate of mirror flexure will be in the range of 4 nm RMS per minute close to the zenith, and approximately 10 nm RMS per minute close to the horizon. The error budget for wavefront sensing corresponds to approximately 25 nm RMS at the zenith and approximately 50 nm RMS close to the horizon. Therefore, the change of mirror figure during a one minute integration represents only a small part of the wavefront sensor error budget.

10. ACKNOWLEDGEMENTS

The authors would like to thank John Roberts and Joe DeVries for preparing figures used in this report, Mike Sheehan for finite-element analysis of telescope structure twisting from elevation drive torque and wind loading, and Rick McGonegal for providing the tracking information for Figure 3.